Cell Reports, Volume *43*

Supplemental information

Reproductive regulation of the mitochondrial stress response in *Caenorhabditis elegans*

Nikolaos Charmpilas, Aggeliki Sotiriou, Konstantinos Axarlis, Nektarios Tavernarakis, and Thorsten Hoppe

Figure S1

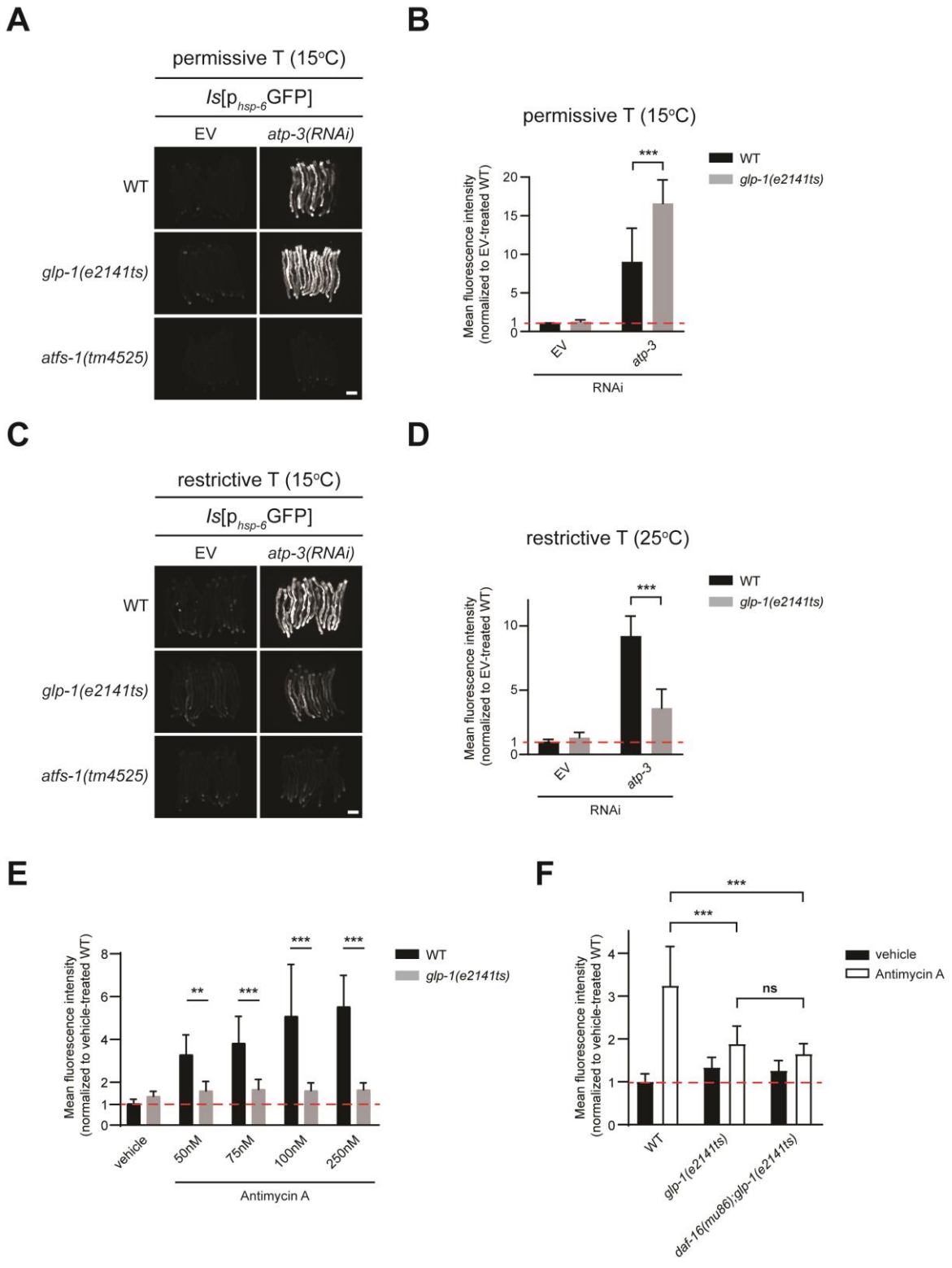

Figure S1: A temperature-sensitive *glp-1* mutation compromises UPR^{mt} inducibility. Related to Figure 1.

A) Photomicrographs of day 3 adult wild-type (WT) and *glp-1(e2141ts)* mutant p$_{hsp-6}$GFP reporter nematodes raised at the permissive temperature (15˚C) and treated with empty vector (EV) and *atp-3(RNAi)* from the L4 larval stage. B) Quantification of intestinal p$_{hsp-6}$GFP fluorescence in WT and *glp-*

1(e2141ts) mutants at the permissive temperature (n=2; ***p<0.001; two-way ANOVA). C) Photomicrographs of day 3 adult WT and *glp-1(e2141ts)* mutant p_{hsp-6}GFP reporter nematodes raised at the restrictive temperature (25˚C) and treated with empty vector (EV) and *atp-3(RNAi)* from the L4 larval stage. D) Quantification of intestinal p_{hsp-6}GFP fluorescence in WT and *glp-1(e2141ts)* mutants at the restrictive temperature (n=2; ***p<0.001; two-way ANOVA). E) Quantification of p_{hsp-6}GFP fluorescence in WT and *glp-1(e2141ts)* mutants upon treatment with increasing concentrations of antimycin A (n=3; ***p<0.001, **p<0.01; two-way ANOVA). F) Quantification of p_{hsp-6}GFP fluorescence in WT, *glp-1(e2141ts)* and *daf-16(mu86); glp-1(e2141ts)* mutants upon treatment with antimycin A (n>3; ***p<0.001; two-way ANOVA). Data are represented as mean ± SD. Scale bars, 200μm.

Figure S2

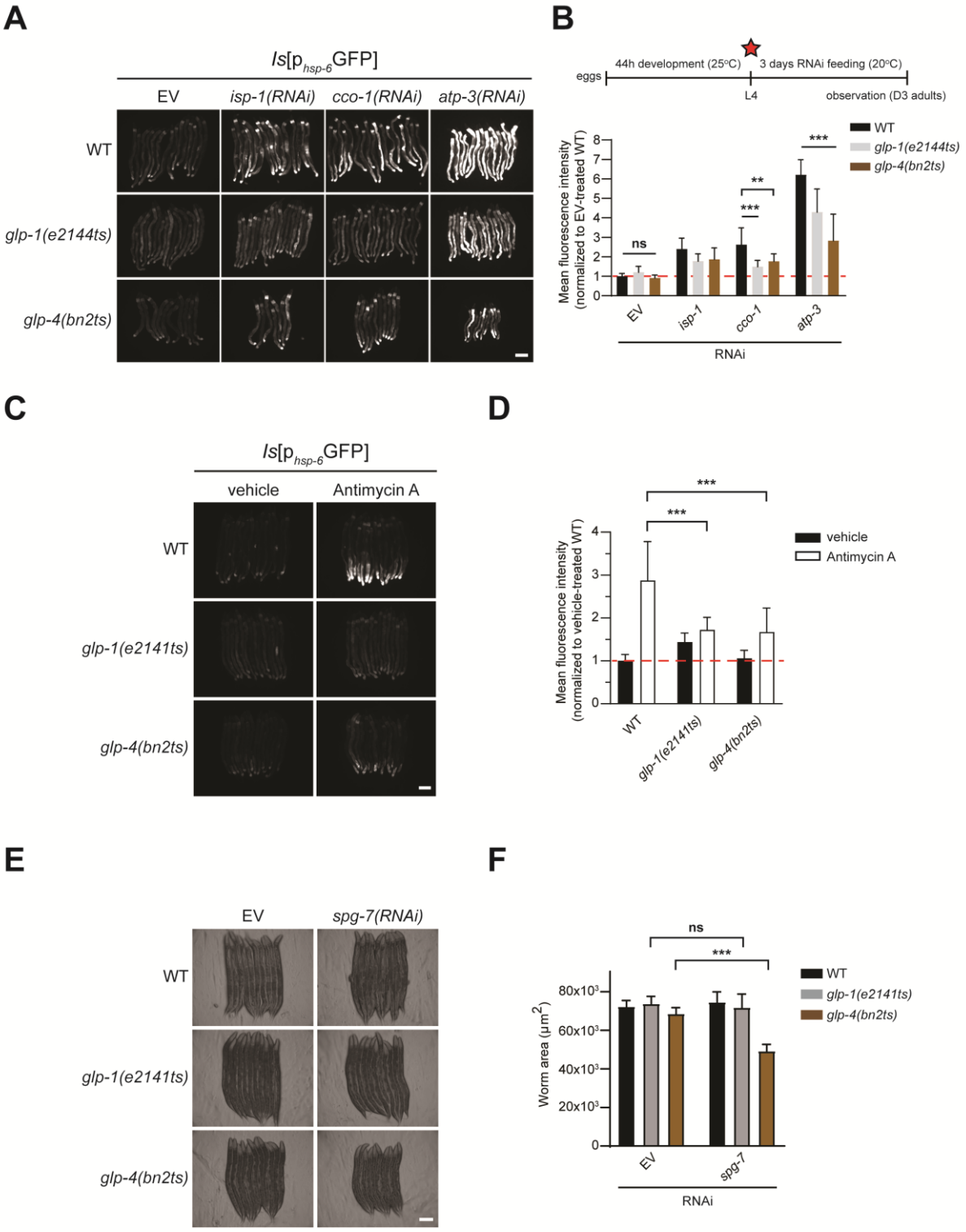

Figure S2: Germline-less *glp-4* mutants are less responsive and vulnerable to mitochondrial stress. Related to Figure 1.

A) Photomicrographs of day 3 adult wild-type (WT), *glp-1(e2144ts)* and *glp-4(bn2ts)* mutant p_{hsp-6}GFP

reporter nematodes treated with empty vector (EV) and three UPR^{mt}-inducing RNAis from the L4 larval stage. B) Quantification of p$_{hsp-6}$GFP fluorescence intensity in WT, *glp-1(e2144ts)* and *glp-4(bn2ts)* mutants (n=3; ***p<0.001, **p<0.01; two-way ANOVA). C) Photomicrographs of day 2 adult WT, *glp-1(e2141ts)* and *glp-4(bn2ts)* mutant p$_{hsp-6}$GFP reporter nematodes treated with antimycin A. D) Quantification of p$_{hsp-6}$GFP fluorescence in WT, *glp-1(e2141ts)* and *glp-4(bn2ts)* mutants upon treatment with antimycin A (n=3; ***p<0.001; two-way ANOVA). E) Photomicrographs of WT, *glp-1(e2141ts)* and *glp-4(bn2ts)* mutants after 72h of feeding with EV or *spg-7(RNAi)* from hatching. F) Quantification of worm surface area (n=2; ***p<0.001; two-way ANOVA). Data are represented as mean ± SD. Scale bars, 200µm.

Figure S3

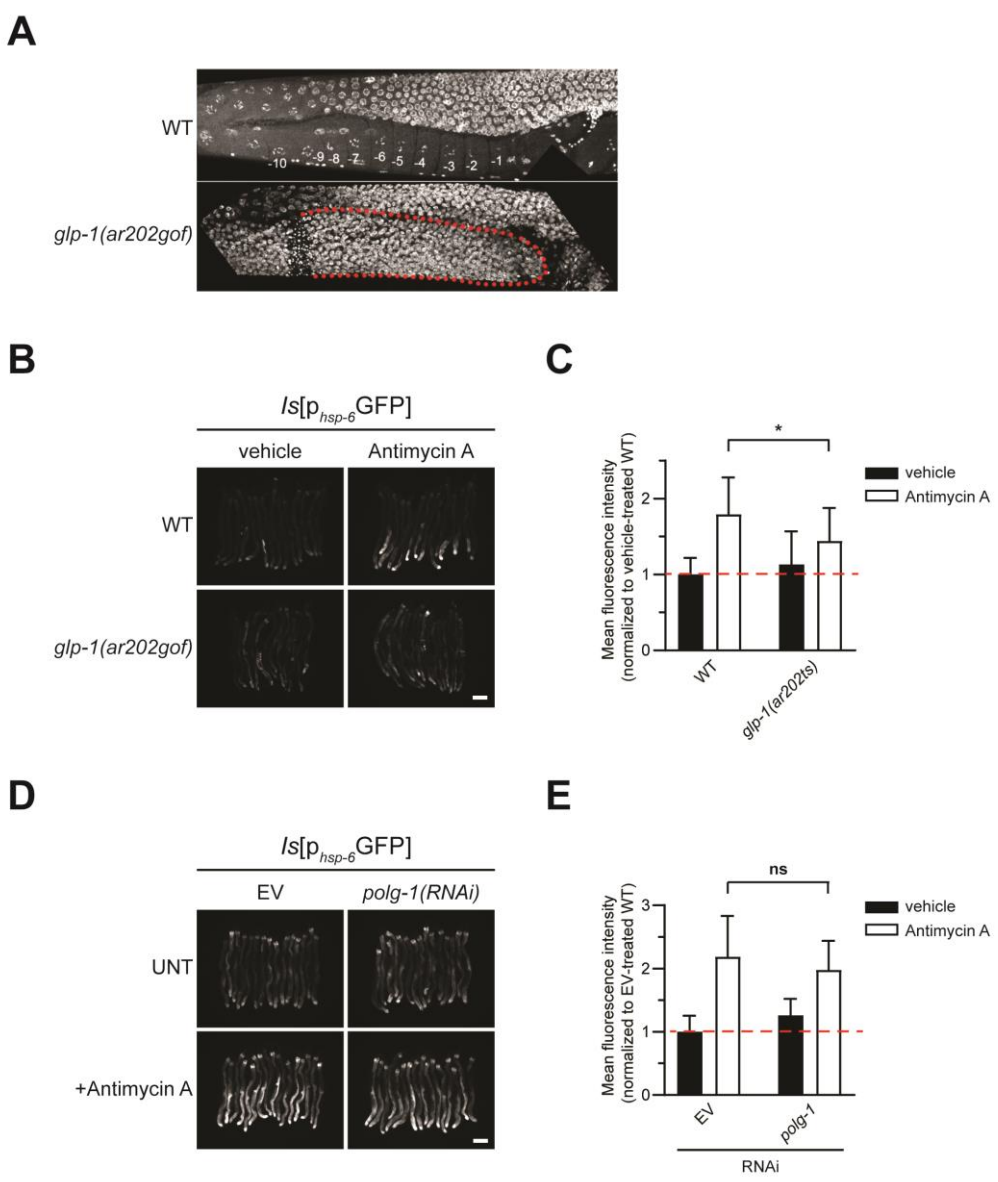

Figure S3: Inhibition of germline stem cell proliferation and reduced mtDNA copy number cannot explain the reduced somatic UPR^{mt} inducibility of germline-less mutants. Related to Figure 2.

A) DAPI staining of WT and *glp-1(ar202gof)* mutant nematodes. The dashed red line surrounds the mitotic cells formed ectopically in the proximal gonad arm of *glp-1(ar202ts)* mutants. B) Photomicrographs of day 2 adult WT and *glp-1(ar202gof)* mutant p$_{hsp-6}$GFP reporter nematodes treated with antimycin A for 24 hours. C) Quantification of p$_{hsp-6}$GFP fluorescence in WT and *glp-1(ar202gof)* mutants upon treatment with antimycin A (n=3; *p<0.05; two-way ANOVA). D) Photomicrographs of day 2 adult p$_{hsp-6}$GFP reporter nematodes raised on empty vector (EV) or *polg-1(RNAi)*-expressing bacteria from hatching and treated at day 1 of adulthood with antimycin A for 24 hours. E) Quantification of p$_{hsp-6}$GFP fluorescence in EV and *polg-1(RNAi)*-treated p$_{hsp-6}$GFP reporter animals upon challenge with antimycin A (n=3; ns p>0.05; two-way ANOVA). Data are represented as mean ± SD. Scale bars, 200µm.

Figure S4

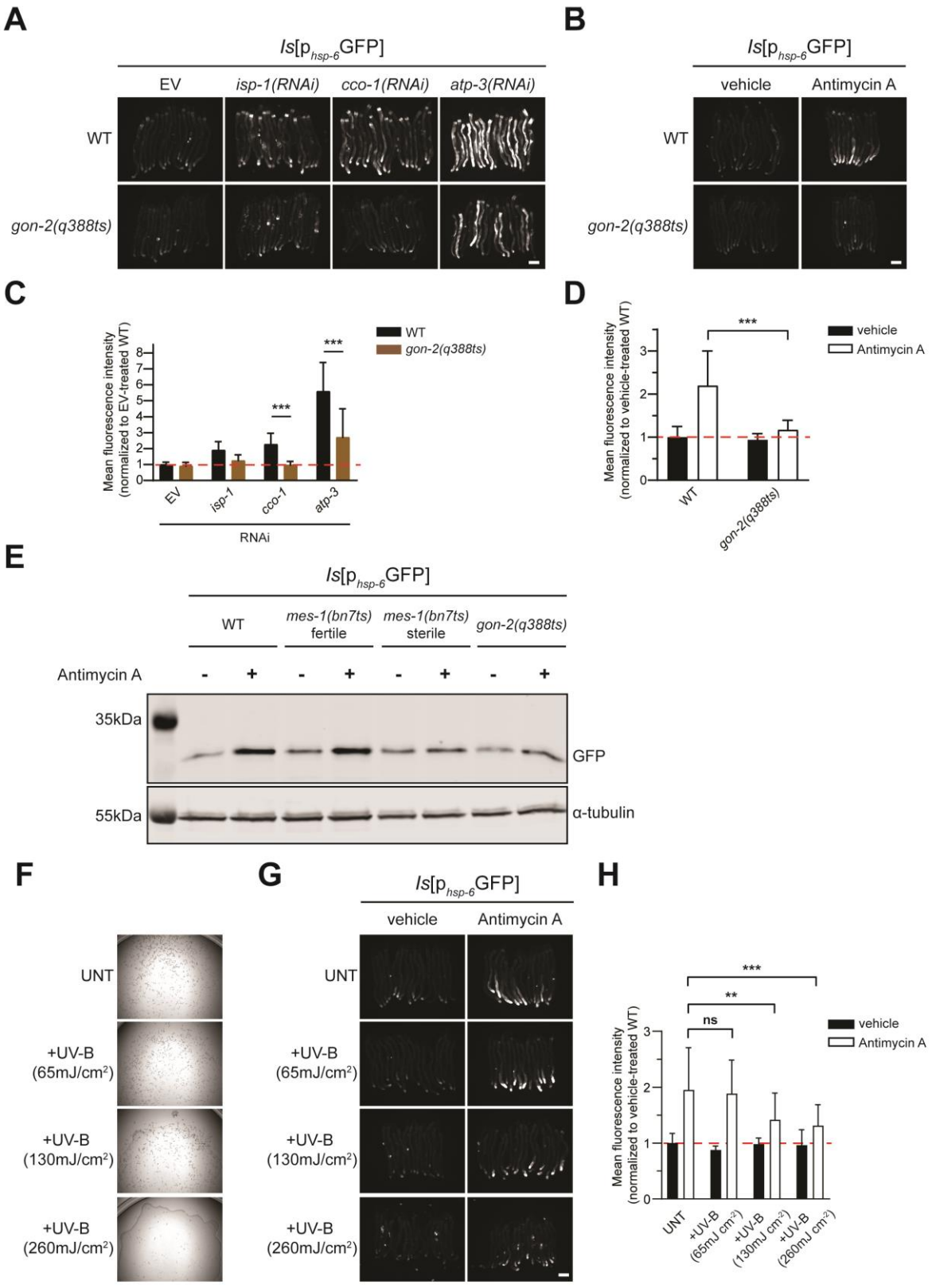

Figure S4: Inhibition of somatic gonad development and UV-B stress lead to reduced somatic UPR^{mt} inducibility. Related to Figure 2.

A) Photomicrographs of day 3 adult WT and *gon-2(q388ts)* mutant p$_{hsp-6}$GFP reporter nematodes treated

with empty vector (EV) and three UPR^{mt}-inducing RNAis from the L4 larval stage. B) Photomicrographs of day 2 adult WT and *gon-2(q388ts)* mutant p$_{hsp-6}$GFP reporter nematodes treated with antimycin A for 24 hours. C) Quantification of p$_{hsp-6}$GFP fluorescence in WT and *gon-2(q388ts)* mutants. Treatments are the same as denoted in (A) (n=3; ***p<0.001; two-way ANOVA). D) Quantification of p$_{hsp-6}$GFP fluorescence in WT and *gon-2(q388ts)* mutants upon antimycin A treatment (n=3; ***p<0.001; two-way ANOVA). E) Western blot for detecting p$_{hsp-6}$GFP in untreated or antimycin A-treated WT, *mes-1(bn7ts)* and *gon-2(q388ts)* mutants. α-tubulin was used as a loading control. F) Exposure to increasing doses of UV-B radiation leads to reduced brood size. G) Photomicrographs of day 2 adult WT p$_{hsp-6}$GFP reporter nematodes exposed to increasing doses of UV-B irradiation prior to the antimycin A challenge. H) Quantification of p$_{hsp-6}$GFP fluorescence intensity upon antimycin A challenge in untreated and UV-B-treated worms (n=3; ***p<0.001, **p<0.01; two-way ANOVA). Data are represented as mean ± SD. Scale bars, 200μm.

Figure S5

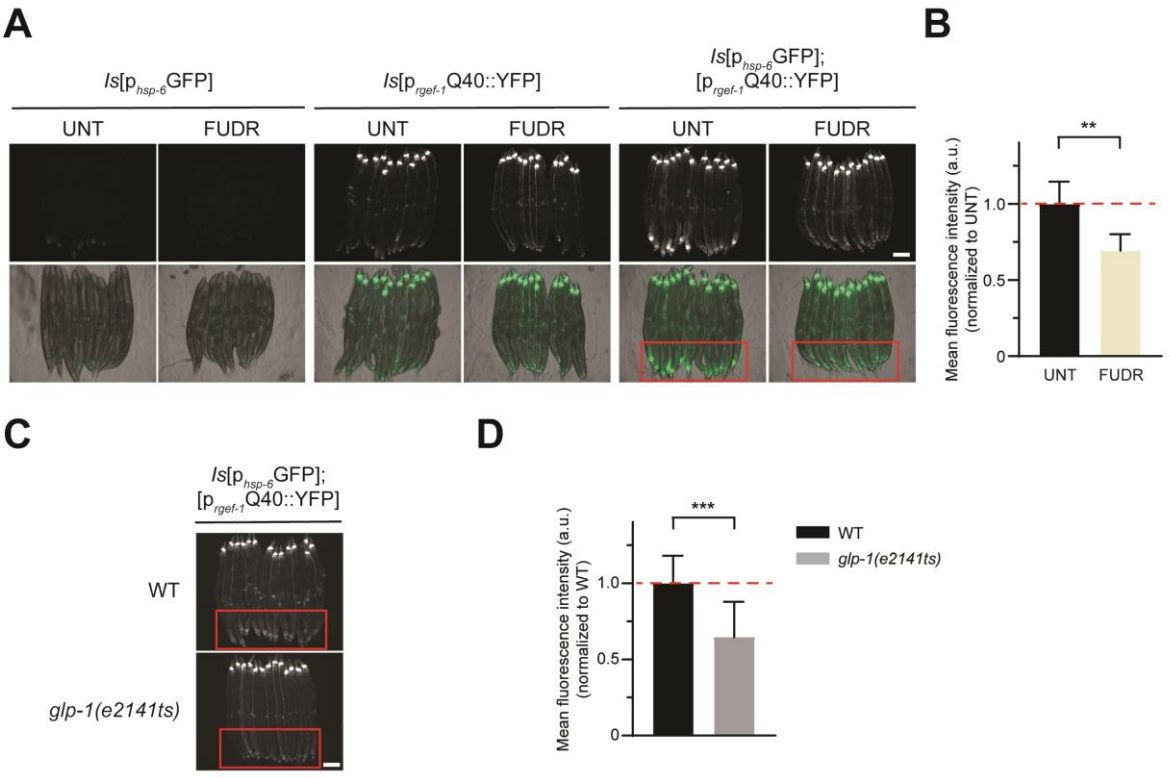

Figure S5: A proliferating germline is required for cell non-autonomous UPR^{mt} induction in response to a panneuronal Q40 polyglutamine tract. Related to Figure 2.

A) Photomicrographs of day 2 adult p_{hsp-6}GFP, p_{rgef-1}Q40::YFP and p_{hsp-6}GFP; p_{rgef-1}Q40::YFP reporter nematodes raised on standard plates or grown on FUDR-containing plates after the L4 larval stage. The red rectangle highlights the posterior intestinal region, where p_{hsp-6}GFP expression is induced in the presence of panneuronal Q40. B) Quantification of p_{hsp-6}GFP fluorescence intensity in untreated and FUDR-treated p_{hsp-6}GFP; p_{rgef-1}Q40::YFP reporter animals (n=3; **p<0.01; two-way ANOVA). C) Photomicrographs of day 2 wild-type and *glp-1(e2141ts)* mutant p_{hsp-6}GFP; p_{rgef-1}Q40::YFP reporter nematodes**.** D) Quantification of p_{hsp-6}GFP fluorescence intensity in p_{hsp-6}GFP; p_{rgef-1}Q40::YFP reporter animals in the absence or presence of the *glp-1(e2141ts)* mutation (n=3; ***p<0.001; two-way ANOVA). Data are represented as mean ± SD. Scale bars, 200µm.

Figure S6

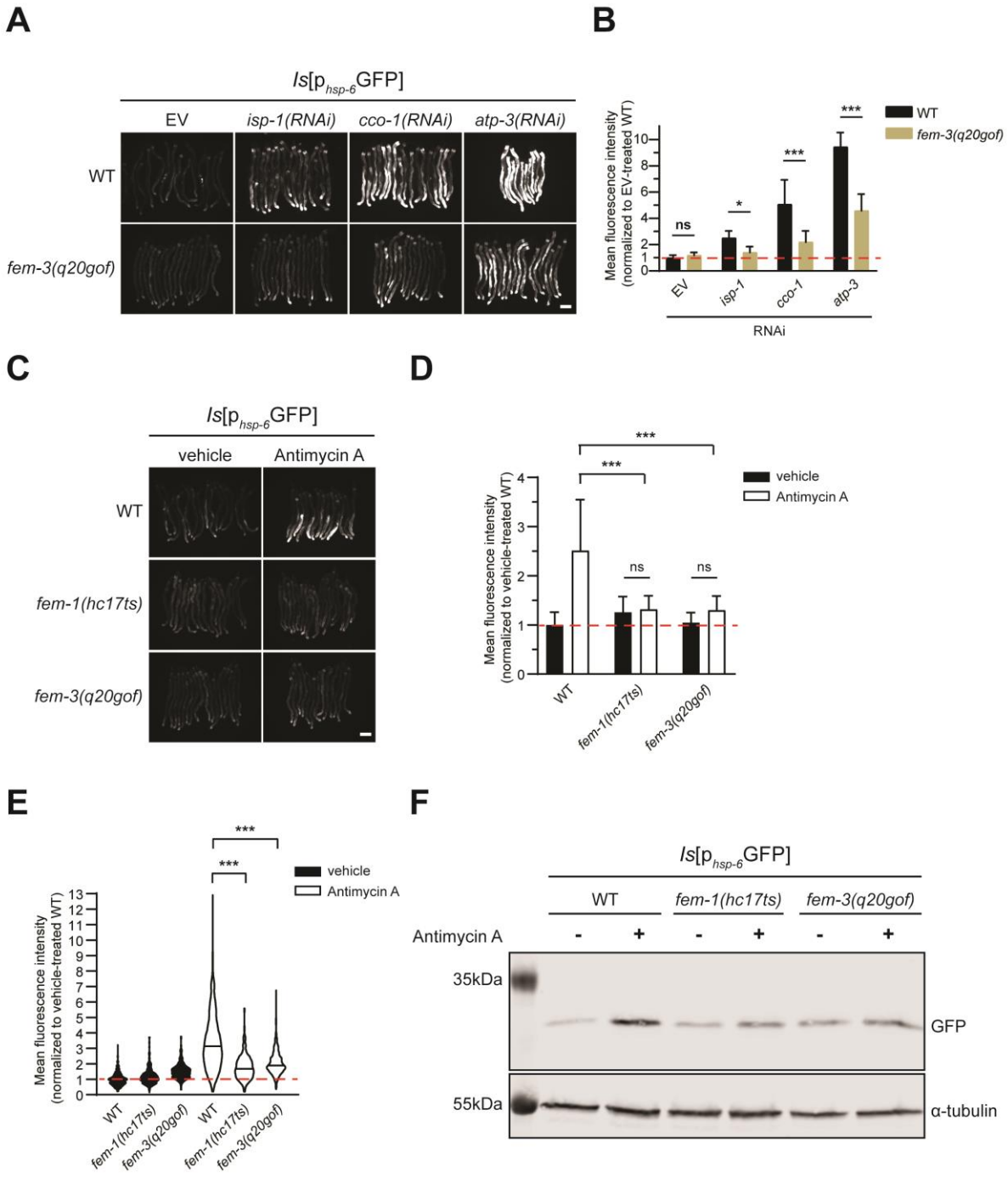

Figure S6: Active reproduction is indispensable for somatic UPR^{mt} induction. Related to Figure 3. A) Photomicrographs of day 3 adult WT and *fem-3(q20gof)* mutant p*hsp-6*GFP reporter nematodes treated with empty vector (EV) and three UPR^{mt}-inducing RNAis from the L4 larval stage. B) Quantification of intestinal p*hsp-6*GFP fluorescence in WT and masculinized mutants (n>3; ***p<0.001, *p<0.05; two-way ANOVA). C) Photomicrographs of day 2 adult WT, *fem-1(hc17ts)* and *fem-3(q20gof)* mutant p*hsp-6*GFP reporter nematodes treated with antimycin A for 24 hours. D) Quantification of p*hsp-6*GFP fluorescence in WT, *fem-1(hc17ts)* and *fem-3(q20gof)* mutants (n>3; ***p<0.001; two-way ANOVA). E) Copas Biosorter quantification of p*hsp-6*GFP fluorescence in WT, *fem-1(hc17ts)* and *fem-3(q20gof)* mutant under

baseline conditions and upon treatment with antimycin A (n=2; ***p<0.001; two-way ANOVA). F) Western blot for detecting $p_{hsp\text{-}6}$GFP in untreated or antimycin A-treated WT, sperm-deficient and oocyte-deficient mutants. α-tubulin was used as a loading control. Data are represented as mean ± SD. Scale bars, 200μm.

Figure S7

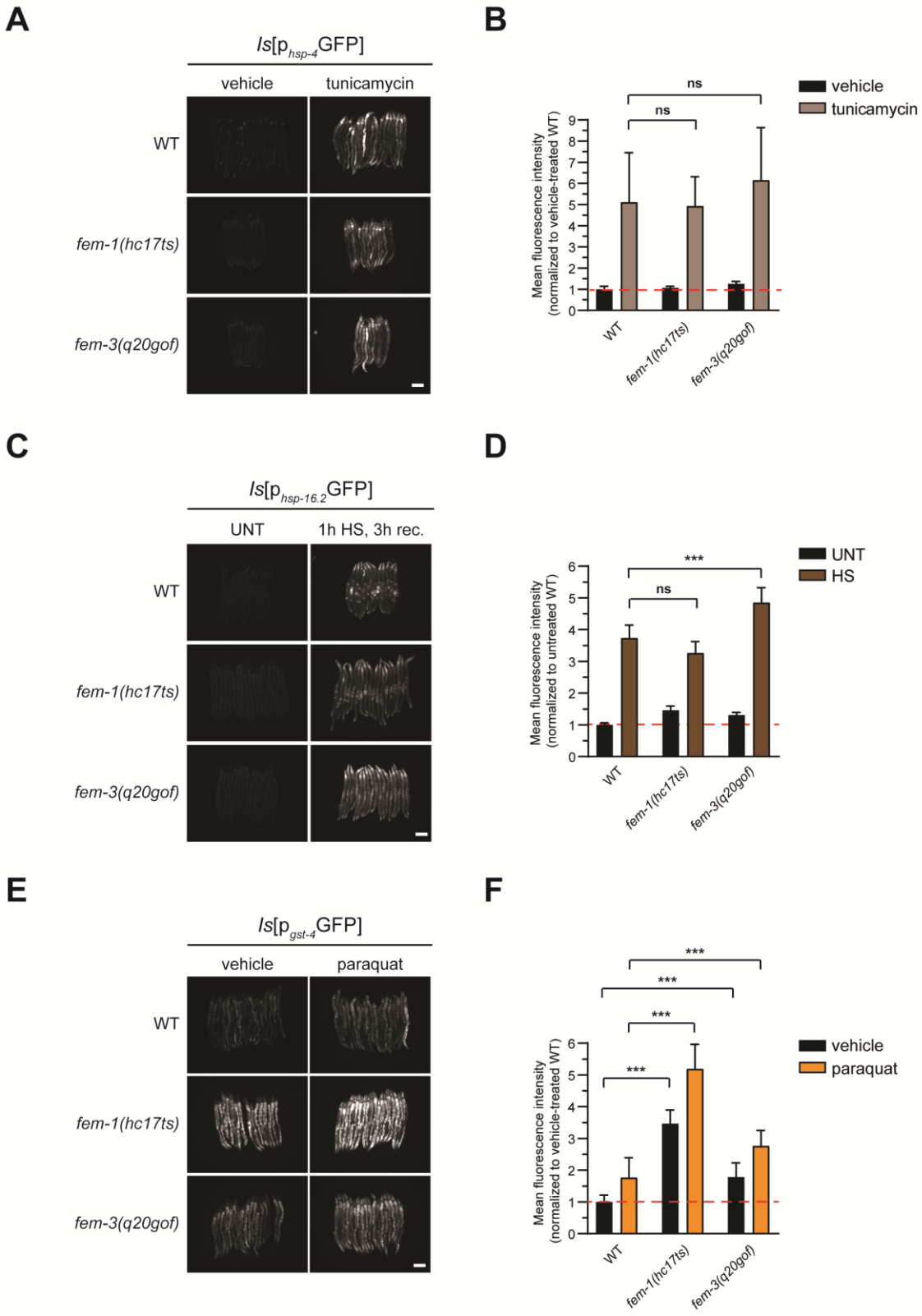

Figure S7: Sperm- and oocyte-deficient mutants can induce the UPR^{ER}, the cytoplasmic HSR and the oxidative stress response. Related to Figure 3.

A) Photomicrographs of day 2 adult WT, *fem-1(hc17ts)* and *fem-3(q20gof)* mutant p$_{hsp-4}$GFP reporter

nematodes treated with vehicle or tunicamycin for 24 hours. B) Quantification of p_{hsp-4}GFP fluorescence in WT, *fem-1(hc17ts)* and *fem-3(q20gof)* mutants (n=3; ns p>0.05; two-way ANOVA). C) Photomicrographs of day 1 adult WT, *fem-1(hc17ts)* and *fem-3(q20gof)* mutant $p_{hsp-16.2}$GFP reporter nematodes upon 1 hour of heat shock at 37˚C followed by a 3-hour recovery. D) Quantification of $p_{hsp-16.2}$GFP fluorescence in WT, *fem-1(hc17ts)* and *fem-3(q20gof)* mutants (n=3; ***p<0.001; two-way ANOVA). E) Photomicrographs of day 2 adult WT, *fem-1(hc17ts)* and *fem-3(q20gof)* mutant p_{gst-4}GFP reporter nematodes treated with vehicle or paraquat for 24 hours. F) Quantification of p_{gst-4}GFP fluorescence in WT, *fem-1(hc17ts)* and *fem-3(q20gof)* mutants (n=3; ***p<0.001; two-way ANOVA). Data are represented as mean ± SD. Scale bars, 200μm.

Figure S8

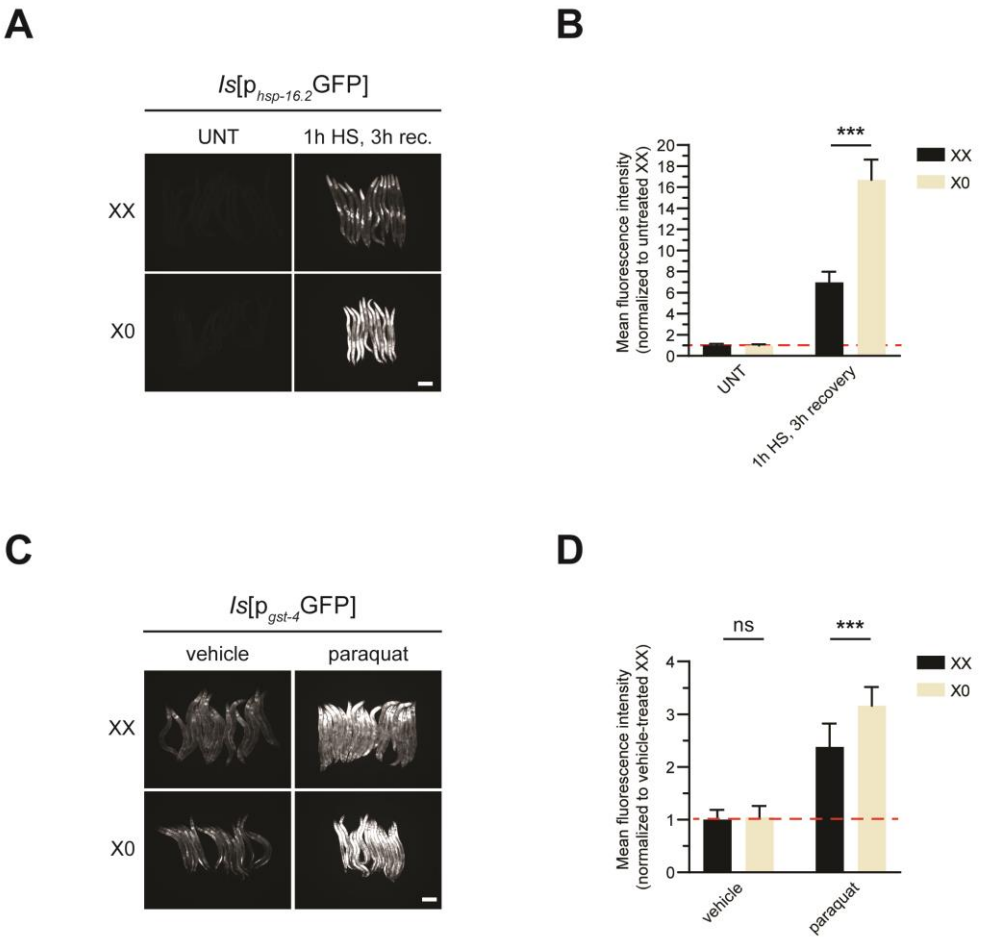

Figure S8: Male nematodes respond to heat shock and oxidative stress. Related to Figure 3.
A) Photomicrographs of day 1 adult hermaphrodite (XX) and male (X0) p*hsp-16.2*GFP reporter siblings upon 1 hour of heat shock at 37˚C followed by a 3-hour recovery. B) Quantification of p*hsp-16-2*GFP fluorescence in wild-type day 1 adult hermaphrodites (XX) and males (X0) upon heat shock (n=3; ***p<0.001; two-way ANOVA). C) Photomicrographs of day 2 adult hermaphrodite (XX) and male (X0) p*gst-4*GFP reporter siblings upon 24-hour exposure to paraquat. D) Quantification of p*gst-4*GFP fluorescence in wild-type day 2 adult hermaphrodites (XX) and males (X0) upon paraquat treatment for 24 hours (n=3; ***p<0.001; two-way ANOVA). Data are represented as mean ± SD. Scale bars, 200µm.

Figure S9

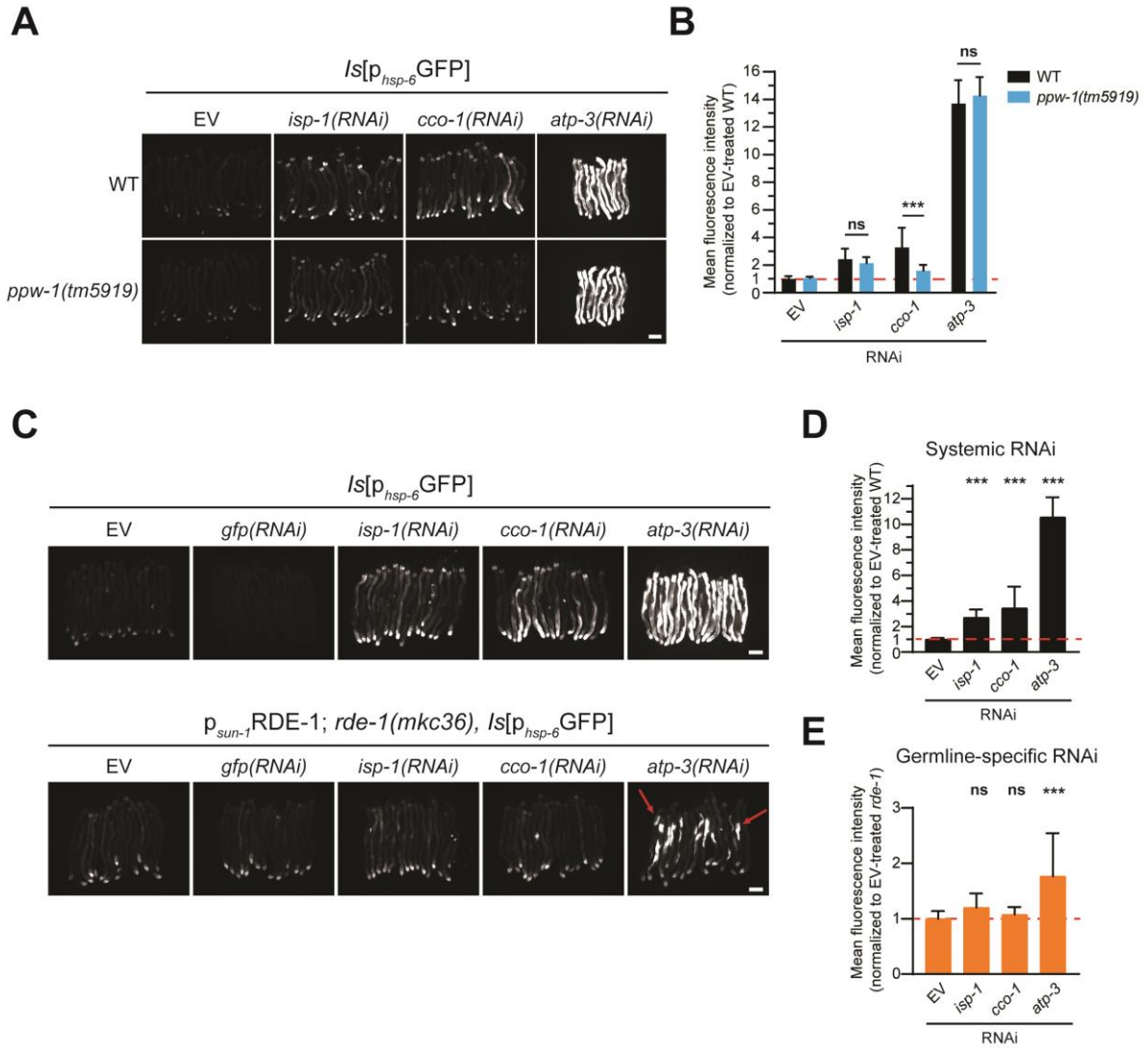

Figure S9: Germline mitochondrial stress induces UPR^{mt} in the soma. Related to Figure 4.

A) Photomicrographs of day 3 adult WT and *ppw-1(tm5919)* mutant p$_{hsp-6}$GFP reporter nematodes treated with empty vector (EV), and three UPR^{mt}-inducing RNAis for three consecutive days from the L4 stage. B) Quantification of intestinal p$_{hsp-6}$GFP fluorescence in WT and *ppw-1(tm5919)* mutant p$_{hsp-6}$GFP reporter nematodes. Treatments are the same as denoted in (A) (n=2; ***p<0.001; two-way ANOVA). C) Photomicrographs of day 3 adult wild-type (WT) and *rde-1(mkc36);p$_{sun-1}$RDE-1* p$_{hsp-6}$GFP reporter nematodes treated with empty vector (EV), *gfp(RNAi)* and three UPR^{mt}-inducing RNAis for three consecutive days from the L4 stage. The red arrows highlight the induction of p$_{hsp-6}$GFP expression in the intestine of *atp-3(RNAi)*-treated *rde-1(mkc36);p$_{sun-1}$RDE-1* p$_{hsp-6}$GFP reporter nematodes. D) Quantification of intestinal p$_{hsp-6}$GFP fluorescence in WT p$_{hsp-6}$GFP reporter nematodes (n=2; ***p<0.001; two-way ANOVA). E) Quantification of intestinal p$_{hsp-6}$GFP fluorescence in *rde-1(mkc36);p$_{sun-1}$RDE-1* p$_{hsp-6}$GFP reporter nematodes (n=2; ***p<0.001; two-way ANOVA). Data are represented as mean ± SD. Scale bars, 200μm.

Figure S10

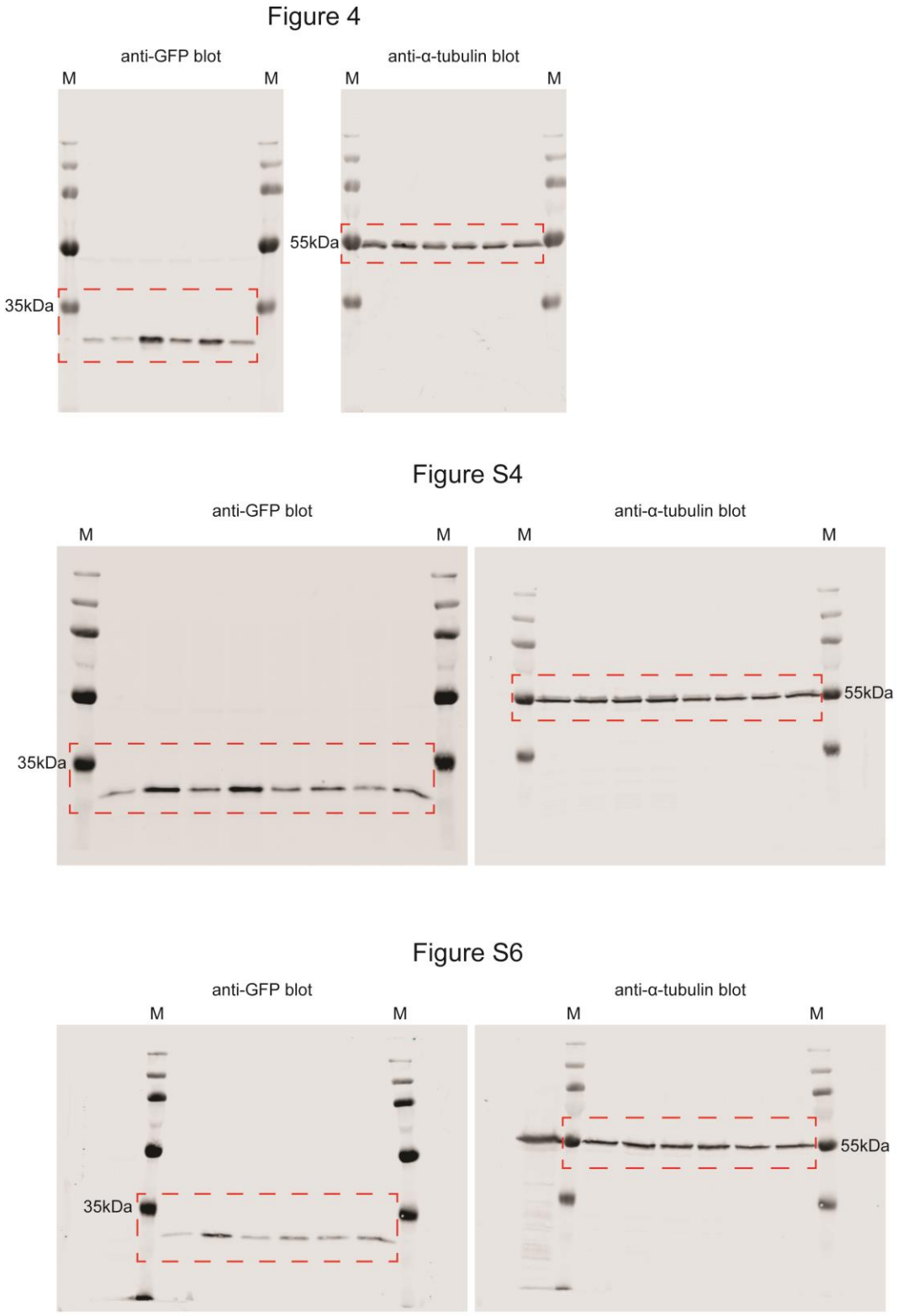

Figure S10: Uncropped protein gels. Related to Figure 4, Figure S4 and Figure S6.
The red dashed rectangles highlight gel areas that were included in the respective figures.